Ocean PHILLS hyperspectral imager: design, characterization, and calibration

Curtiss O. Davis, Jeffrey Bowles, Robert A. Leathers, Dan Korwan, T. Valerie Downes, William A. Snyder, W. Joe Rhea, Wei Chen

Naval Research Laboratory, Code 7212, 4555 Overlook Ave. S. W., Washington, D. C. 20375
davis@rsd.nrl.navy.mil, jeffrey.bowles@nrl.navy.mil, leathers@rsd.nrl.navy.mil, korwan@poamb.nrl.navy.mil,
downes@rsd.nrl.navy.mil, snyder@rsd.nrl.navy.mil, rhea@rsd.nrl.navy.mil, chen@rsd.nrl.navy.mil
http://rsd-www.nrl.navy.mil/7212

John Fisher

Brandywine Optical Technologies, P O. Box 459, West Chester, PA 19381
brandywine.optics@verizon.net

W. Paul Bissett

Florida Environmental Research Institute,
4807 Bayshore Blvd., Tampa, FL 33611
pbissett@flenvironmental.org

Robert Alan Reisse

Science Inquiries, Inc., 312 Patleigh Road, Catonsville, MD 21228
rareisse@postoffice.worldnet.att.net

Abstract: The Ocean Portable Hyperspectral Imager for Low-Light Spectroscopy (Ocean PHILLS) is a hyperspectral imager specifically designed for imaging the coastal ocean. It uses a thinned, backside-illuminated CCD for high sensitivity and an all-reflective spectrograph with a convex grating in an Offner configuration to produce a nearly distortion-free image. The sensor, which was constructed entirely from commercially available components, has been successfully deployed during several oceanographic experiments in 1999-2001. Here we describe the instrument design and present the results of laboratory characterization and calibration. We also present examples of remote-sensing reflectance data obtained from the LEO-15 site in New Jersey that agrees well with ground-truth measurements.

©2002 Optical Society of America

OCIS Codes: (010.4450) ocean optics, (120.0280) remote sensing, (300.6550) visible spectroscopy

---

References and Links

1. A. F. H. Goetz, G. Vane, J. E. Solomon, and B. N. Rock, "Imaging spectrometry for Earth remote sensing," Science **228**, 1147-1153 (1985).
2. Z. Lee, K. L. Carder, R. F. Chen, and T. G. Peacock, "Properties of the water column and bottom derived from Airborne Visible Infrared Imaging Spectrometer (AVIRIS) data," J. Geophys. Res. **106**, 11639-11651 (2001).
3. S. Sathyendranath, D. V. Subba Rao, Z. Chen, V. Stuart, T. Platt, G. L. Bugden, W. Jones, and P. Vass, "Aircraft remote sensing of toxic phytoplankton blooms: a case study from Cardigan River, Prince Edward Island," Can. J. Remote Sens. **23**, 15-23 (1997).
4. P. J. Mumby, J. R. M. Chisholm, C. D. Clark, J. D. Hedley, and J. Jaubert, "A bird's-eye view of the health of coral reefs," Nature **413**, 36 (2001).
5. T. L. Wilson and C. O. Davis, "Hyperspectral Remote Sensing Technology (HRST) program and the Naval EarthMap Observer (NEMO) satellite," in Infrared Spaceborne Remote Sensing VI, M. S. Scholl and B. F. Andresen, eds., Proc. SPIE **3437**, 2-10, (1998).
6. T. L. Wilson and C. O. Davis, "The Naval EarthMap Observer (NEMO) Satellite," in Imaging Spectrometry V, M. R. Descour and S. Shen, eds., Proc. SPIE **3753**, 2-11 (1999).
7. J. Bowles, M. Kappus, J. Antoniades, M. Baumback, M Czarnaski, C. O. Davis, and J. Grossmann, "Calibration of inexpensive pushbroom imaging spectrometers," Metrologica **35**, 657-661 (1998).

8. R. O. Green, M. L. Eastwood, C. M. Sarture, T. G. Chrien, M. Aronsson, B. J. Chippendale, J. A. Faust, B. E. Pavri, C. J. Chovit, M. S. Solis, M. R. Olah, and O. Williams, "Imaging spectroscopy and the Airborne Visible Infrared Imaging Spectrometer (AVIRIS)," Remote Sens. Environ. **65**, 227-248 (1998).
9. R. G. Resmini, M. E. Kappus, W. S. Aldrich, J. C. Harsanyi, and M. Anderson, "Mineral mapping with HYperspectral Digital Imagery Collection Experiment (HYDICE) sensor data at Cuprite, Nevada, USA," Int. J. Remote Sens. **18**, 1553-1570 (1997).
10. Office of Naval Research (ONR) Coastal Benthic Optical Properties (CoBOP) program, http://www.psicorp.com/cobop/cobop.html.
11. Hyperspectral Coupled Ocean Dynamics Experiments (HyCODE), http://www.opl.ucsb.edu/hycode.html.
12. Florida Environmental Research Institute, http://www.flenvironmental.org/Projects.htm.
13. Long-term Ecosystem Observatory at a 15 Meter Depth (LEO-15), http://marine.rutgers.edu/mrs/LEO/LEO15.html.
14. J. Fisher, J. A. Antoniades, C. Rollins, and L. Xiang, "Hyperspectral imaging sensor for the coastal environment," in International Optical Design Conference 1998, L. R. Gardner and K. P. Thompson, eds., Proc. SPIE **3482**, 179-186 (1998).
15. J. Fisher, M. M. Baumback, J. H. Bowles, J. M. Grossmann, and J. A. Antoniades, "Comparison of low-cost hyperspectral sensors," in Imaging Spectrometry IV, M. R. Descour and S. S. Shen, eds., Proc. SPIE **3438**, 23-30 (1998).
16. H. Gumbel, "System considerations for hyper/ultra spectroradiometric sensors," in Hyperspectral Remote Sensing and Applications, S. S. Shen, ed., Proc. SPIE **2821**, 138-170 (1996).
17. A. Offner, "Annular field systems and the future of optical microlithography," Opt. Eng. **26**, 294-299 (1987).
18. P. Mouroulis, R. O. Green, and T. G. Chrien, "Design of pushbroom imaging spectrometers for optimum recovery of spectroscopic and spatial information," Appl. Opt. **39**, 2210-2220 (2000).
19. R. A. Leathers, T. V. Downes, W. A. Snyder, J. H. Bowles, C. O. Davis, M. E. Kappus, M. A. Carney, W. Chen, D. Korwan, M. J. Montes, and W. J. Rhea, Ocean PHILLS Data Collection and Processing: May 2000 Deployment, Lee Stocking Island, Bahamas, U. S. Naval Research Laboratory technical report NRL/FR/7212--01-10,010 (in press).
20. B.-C. Gao, M. J. Montes, Z. Ahmad, and C. O. Davis, "Atmospheric correction algorithm for hyperspectral remote sensing of ocean color from space," Appl. Opt. **39**, 887-896 (2000).
21. M. J. Montes, B.-C. Gao, and C. O. Davis, "A new algorithm for atmospheric correction of hypespectral remote sensing data," in Geo-Spatial Image and Data Exploitation II, W. E. Roper, ed., Proc. SPIE **4383**, 23-30 (2001).

1. Introduction

Optical remote sensing of coastal oceanic waters is key to Naval systems for bathymetry, mine hunting, submarine detection, and submerged hazard detection. Visible radiation is the only portion of the electromagnetic spectrum that directly probes the water column, and visible imaging systems show great promise for meeting Naval requirements in the littoral ocean. In particular, hyperspectral imagers, also called imaging spectrometers because they collect a continuous spectra for each pixel in the image [1], are proving to be particularly useful for resolving the complexity of the coastal ocean environment [2]. Hyperspectral remote sensing is also proving useful for the monitoring of large-scale coastal environmental conditions, such as biological primary production, coral reef health, harmful algal blooms, and anthropogenic impacts [e.g., 3,4]. To support the development of these applications and to test design features for the Coastal Ocean Imaging Spectrometer (COIS) to be flown on the Naval Earth Map Observer (NEMO) spacecraft [5,6], we have designed, built, and deployed the Ocean Portable Hyperspectral Imager for Low-Light Spectroscopy (Ocean PHILLS) instrument.

Over the past eight years the Naval Research Laboratory (NRL) has built a series of PHILLS hyperspectral imagers. Bowles, *et al.* [7] describes three of the earlier PHILLS cameras and their calibration and characterization. NRL started development of these instruments in 1994. At that time un-intensified cameras were not sensitive enough for spectrally imaging the ocean, which is a very dark target. The first PHILLS instruments used intensified cameras to deal with these low-light conditions. These instruments provided great sensitivity, but they suffered from relatively low signal-to-noise ratios (SNR) and poor dynamic range. The poor dynamic range led to the use of auto-iris systems, but the unstable nature of intensified cameras and the difficulty in tracking the rapidly changing auto-iris setting made calibration of these systems problematic. The recent availability of thinned, backside-illuminated detector arrays with greater sensitivity, particularly in the blue region of

the spectrum, have enabled us to overcome these problems. Early versions of the PHILLS camera were analog and were limited to a standard video format of 640 across-track pixels. Development of larger format detector arrays (the NRL Ocean PHILLS-1 currently contains a detector with 1024 across-track pixels) have extended the flexibility of designing high resolution, high signal-to-noise imaging spectrometers, allowing for wider swaths and higher spectral resolution, even for low albedo scenes such as the coastal ocean.

Other airborne hyperspectral sensors have been deployed in recent years, most notably the AVIRIS (Airborne Visible/Infrared Imaging Spectrometer) [8] and the HYDICE (Hyperspectral Digital Imagery Collection Experiment) [9] sensors. Both are one-of-a-kind sensors supported by large, dedicated programs. Both sensors have proven useful for many applications including oceanography, but have been difficult to schedule due to many competing user requirements. By comparison, the Ocean PHILLS is a compact light-weight system that is constructed from commercially available components at a relatively low cost. This has made it possible to produce multiple copies of the ocean PHILLS that are dedicated to various Naval research programs.

The Ocean PHILLS in its various forms of development has been deployed during several coastal oceanographic experiments. Recent deployments include those as part of the Coastal Benthic Optical Properties (CoBOP) program [10] at Lee Stocking Island, Bahamas (May/June 1999 and May 2000) and as part of the Hyperspectral Coupled Ocean Dynamics Experiments (HyCODE) program [11] on the West Florida Shelf [12] (2000 and 2001) and at the LEO-15 site [13] in New Jersey (July 2000 and July 2001). These were all part of multi-institutional experiments that involved a large amount of ground-truth measurements of land, water, and seafloor optical properties. These data sets are being used to develop algorithms for a variety of applications for the coastal ocean and adjacent land areas.

This paper describes the Ocean PHILLS instrument in its present form and the results of laboratory calibration and characterization. Example data are provided from the 2001 deployment at LEO-15.

2. Ocean PHILLS system design

The Ocean PHILLS is a pushbroom-scanning instrument. A camera lens is used to image a ground scene onto a narrow slit that is the entrance to the spectrometer. The slit acts as a field stop, allowing only light from along a line on the ground to enter the spectrometer. The light passing through the slit is dispersed by the spectrograph onto a 2-dimensional charged-coupled device (CCD) detector array. The image of the ground projected through the slit is aligned along one dimension of the CCD (the cross-track spatial direction) and the spectrum of each spatial pixel is dispersed along the other dimension of the CCD (the spectral direction). The second spatial dimension of the scene is then constructed as the sensor platform (typically an aircraft) moves forward in the along-track direction, causing the image projected on the slit to change continuously as the camera acquires new frames of data. This results in a three-dimensional image "cube" with two spatial dimensions and one spectral dimension. The instantaneous field of view (IFOV) is determined by the fore-optics of the system. Typically, the Ocean PHILLS systems use IR compensated (400-1000 nm) lenses (Schneider Optics, Inc) with focal lengths of 12, 17, or 23 mm, resulting in IFOV's of 10 mrad, 7.1 mrad and 5.2 mrad, respectively. The ground sample distance (GSD) in the along-track direction is the product of the integration time and aircraft ground speed. The cross-track GSD is given by the product of the magnification of the system and the detector pixel pitch. Because the spectrograph used in the PHILLS provides unit magnification, the ratio of the aircraft altitude to the focal length of the fore-optics determines the magnification of the system.

The HyperSpec™ spectrograph was designed collaboratively by the NRL and American Holographic, Inc. (now Agilent Technologies, Fitchburg, MA) to produce high throughput, low distortion, and high image quality. A grating imaging spectrograph was chosen for its advantages over other hyperspectral technologies such as those incorporating prism, wedge filter, and interferometric techniques [14,15,16]. The main limitations that traditional grating-

based systems have encountered are optical distortions when using apertures f/4 and faster, stray light from multiple diffraction orders, and sensitivity to polarization of the incoming light. The primary advantages of a grating design over filter approaches are the simultaneity in acquisition of each spectrum and higher spectral resolution. This greatly simplifies post-flight data processing for aircraft data. Because transmission holographic gratings have difficulties achieving the low distortion and stray light required for the Ocean PHILLS, a reflective surface grating was chosen. The optical distortions typically associated with imaging spectrographs are the change of dispersion angle with field position (smile) and change of magnification with spectral channel (spectral keystone). These distortions affect spectral purity and thus limit the robustness of subpixel demixing and detection algorithms. The HyperSpec™ VS-15 spectrograph avoids these problems by using an Offner Spectrograph [17] with an astigmatism-corrected reflective diffraction grating (Figure 1). The Offner spectrograph design has inherently low smile and keystone distortion [17, 18]. The design was optimized by selecting mirror tilts and the grating's holographic construction point positions to balance third- and fifth-order astigmatism. The spectrograph was designed with a groove density of 55 grooves/mm. Although the spectrograph design is telecentric (with the entrance pupil at infinity), standard C-mount 2/3 inch format video lenses which are not telecentric are used for the ocean PHILLS. Vignetting has been avoided in this configuration by operating the system at an f-stop of f/4 or greater. By allowing the lens iris to be the system stop at f/4, the spectrograph is no longer telecentric but has its entrance pupil at the exit pupil of the lens.

HyperSpec™ VS-15 Specifications	
Size	180 x 150 x 150 mm
Weight	24 oz. (w/o camera or lens)
Field size	12 mm
Dispersion	400–1000 nm over 6 mm
Aperture	f/2
Spot size	< 24 μm rms
Keystone Distortion	< 0.1%
Smile Distortion	< 0.1%

1 – lens 4 – convex grating
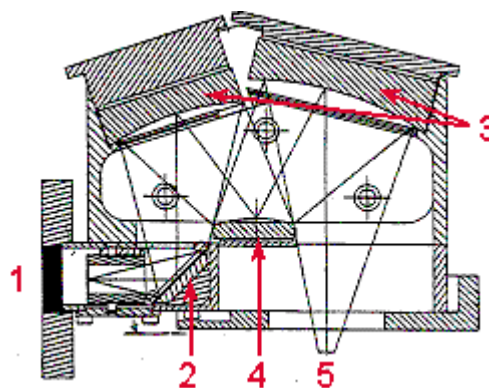2 – fold mirror 5 – CCD camera
3 – concave mirrors

Figure 1. Design and specifications for the HyperSpec™ VS-15 Offner Spectrograph.

The primary selection criteria for the camera were a frame rate of >30 Hz, high quantum efficiency in the blue (400 - 450 nm), large dynamic range, and low noise. The desired format was at least 640 pixels across track by at least 120 spectral channels. Thinned, backside-illuminated, split frame-transfer, multiple readout CCD cameras from PixelVision Inc. (Beaverton, OR) were selected. Cameras sold by PixelVision include a 494X652 4-readout format, and a 1024X1024 4-readout format. Both these cameras are arranged in a four quadrant configuration to provide multiple taps for higher readout rates. They have a 12 μm pixel size, a low readout noise specification (~30 electrons), sufficient well depth, and a true 14-bit readout to meet our SNR and dynamic range requirements. The spectrometer disperses the 400 - 1000 nm spectral region over approximately 6 mm. The full array is used in the smaller format camera (652 spatial samples, 494 spectral channels), but only one half of the

array is used for the larger format camera (1024 spatial samples, 512 spectral channels). The pixels in the spectral direction are normally binned by four on the CCD chip to yield 124 or 128 spectral channels, each approximately 4.6 nm wide. The CCD is thinned and backside-illuminated, allowing the photons to enter the active region without passing through the polysilicon gates. Avoiding these gates, which are strong absorbers of blue light, allows very high quantum efficiencies (on the order of 50-80%). The thin uniform layer of silicon on the backside also allows the use of an anti-reflective coating. Other attributes of the detector considered in characterization and calibration were the different offsets and gains for the two or four outputs of each readout, or tap, and frame-transfer smear. Tests showed that these potential artifacts from readout and frame transfer do not adversely affect the overall sensor performance or the scientific value of the data to any measurable degree.

If left unblocked, the second order diffraction pattern from the shorter wavelengths (380 nm – 500 nm) falls on the detector array in the active area used to measure the first order pattern of the longer wavelengths (760 nm – 1000 nm). Therefore, a UV/blue absorption filter was placed on the camera window, behind the spectrometer, to block that second order light. The filter blocks wavelengths shorter than 530 nm. It is placed on the camera entrance window in such a way that it covers the pixels used to detect wavelengths above 590 nm. Because several mm separate the filter from the detector, the system is operated with the camera lens set to f/4 or higher to insure no second order light bypasses the filter.

In deployments of the PHILLS prior to 2001, some of the zero-order portion of the diffraction pattern was scattering inside of the spectrometer and contaminating the data. In particular, zero order light was scattering off of a black anodized aluminum C-mount ring surrounding the camera window and scattering onto the CCD in a distinct flaring pattern. The centers of the zero-order peaks were closer to the center of the array at high channel numbers than at low channel numbers. This pattern could be seen in across-sample profiles of the blue-wavelength channels of radiometric calibration data. The PHILLS was modified prior to the 2001 deployments by placing a flat-black mask over the camera window to block this zero-order light and subsequent data shows that the alteration was successful. For data sets prior to 2001 this zero-order light artifact is removed during data processing [19].

A Microsoft Windows NT-based personal computer (PC) controls the camera through a PCI interface card. All digitization of the signal occurs at the camera and the data are communicated to the computer through fiber optic cables. PixelVision provides a Software Development Kit (SDK) that allows low-level control of the camera. Software developed by the NRL configures the camera for the particular mode desired, including high or low gain, frame rate, and number of frames to collect. The computer then "grabs" data from the camera and writes it to a hard disk in a standard file format. Data rates are typically less than 7.5 MB/s. A data "run" consists of data taken while the plane flies in a line. A flight line may be flown for as long as 15 minutes and the corresponding data run may contain several gigabytes of data. The data is routinely viewed immediately after the run is finished to check data quality and is later written to tape for archiving.

In the aircraft the instrument is mounted on vibration dampening mounts. Geolocation of the collected PHILLS data is derived with data collected from a Global Positioning Satellite/Inertial Navigational System (GPS/INS) system mounted on the same base plate as the camera. The aircraft location (latitude, longitude and altitude) and pointing information (pitch, roll, and heading) are measured at a frequency of 10 Hz. Both the camera data and the GPS/INS data have time tags that allow them to be temporally matched during post-processing.

3. Characterization and calibration

Hyperspectral sensor characterization can be divided into the broad areas of image quality, spectral fidelity, and radiometric performance. Image quality figures of merit include spot size and distortion. Spectral quality can be specified in terms of optical distortions or imperfections (smile or keystone distortion and blur), area artifacts (stray light, ghost reflections, multiple orders, and frame transfer smear), and linearity. Radiometric performance includes linearity, signal-to-noise ratio, dynamic range, and temporal and thermal stability.

3.1 Image quality

The spatial performance was measured with a near-field target containing spectral lines, in this case a fluorescent tube masked with a bar pattern (Figure 2, Table 1). A measure of the image quality was obtained by fitting a Gaussian to the shape of the image at the edges of the bar target. The FWHM of the Gaussian was then used as the metric for the optical performance of the system. Imaging a point source would be a more accurate measure and will be performed at a later date. For an aperture of f/4, the FWHM was estimated to be approximately 3 pixels.
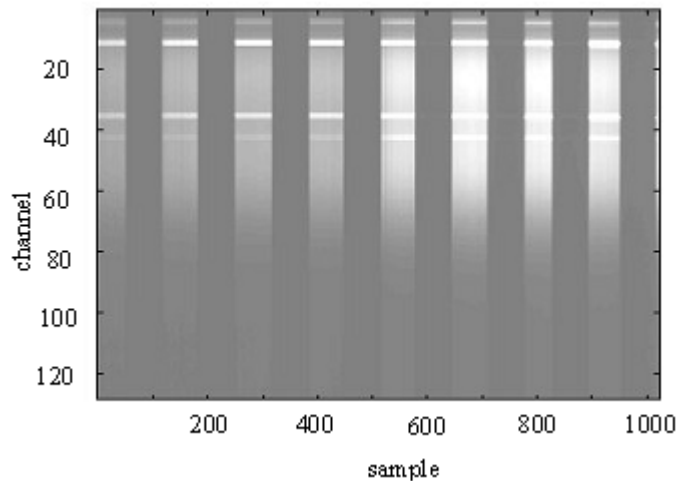

Figure 2. Spatial image of the bar target showing 1024 spatial channels (horizontal) and 128 (512 binned by 4) spectral channels (vertical dimension). The non-uniformity from the top to the bottom is due to the spectral properties of the light source which is blue rich and has spectral emission lines.

Table 1. Measured spatial performance metrics for the complete PHILLS, including lens, spectrograph, and camera.

Performance Metric at f/4	Value
RMS Spot size (spatial direction)	3 unbinned pixels (36 μm)
RMS Spot size (spectral direction)	2 unbinned pixels (24 μm)
Keystone Distortion	< 1 unbinned pixel
Smile Distortion	< 1 unbinned pixel

3.2 Spectral fidelity

The spectral attributes for the sensor were determined from measurements of laser light and gas discharge lamps. The laser measurements identify the spectral response function of the detector as well as the spectral stray light (on the order of 10^{-4} of the signal from outside the IFOV falling on the IFOV), which is characteristic of a single monochromater-like system. The gas discharge lamp measurements, which are also used for spectral calibration, provide a measure of the linearity of the spectral dispersion. Both experiments provide tests for rotation and for keystone and smile distortions.

The laser experiments were performed with 543.5 nm (green), 594.1 nm (yellow), and 632.8 nm (red) helium-neon lasers. The laser beam was projected through a 16X microscope objective to spread the beam over a larger area and then passed through a ground glass diffuser. The spectrometer lens was placed directly behind the diffuser. Measurements were taken both with and without binning the spectral direction, resulting in either 128 or 512 spectral bands. Multiple frames of data were taken and averaged together to reduce noise effects when analyzing this data. Additionally, camera offset levels, measured by taking data when there is no input to the spectrometer, were subtracted from the illuminated data. Shown in Figure 3 is a measured spectrum of the 594.1 nm laser. The spectral response shape is approximately that of a Gaussian near the illumination wavelength (Figure 3 inset). Away from the illumination wavelength there is a nearly constant stray light value that is on the order of 0.01% of the peak value. Results for the other laser wavelengths were similar to those for 594.1 nm.
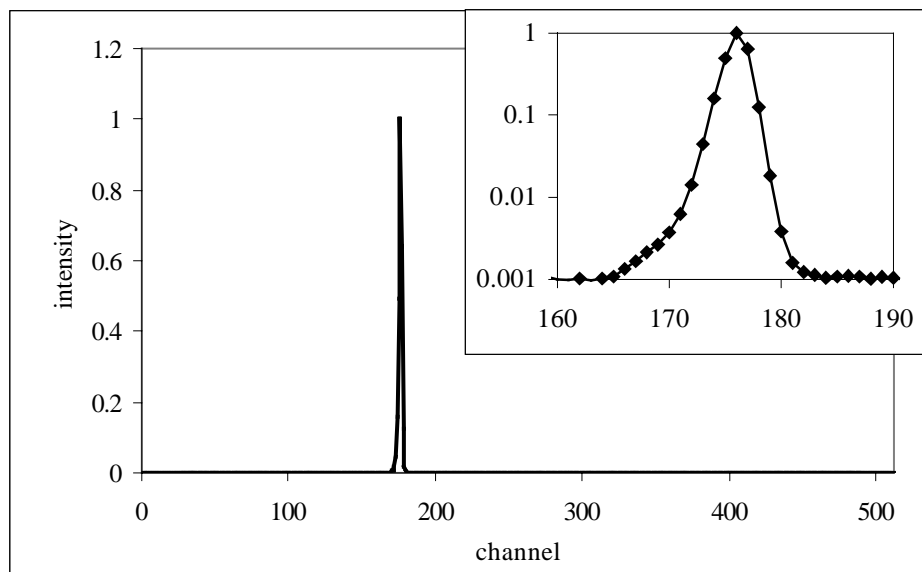

Figure 3. The spectral response of the PHILLS to 594.1 nm Helium-Neon laser light. The data are unbinned with a channel width of 1.15 nm. The inset figure is a close-up view for channels near the spectral peak plotted on a logarithmic scale.

Spectral calibration is performed by imaging several different gas emission lamps (oxygen, mercury, argon, helium) reflected off a diffuse surface. For these measurements the camera is set up so that it does not bin the data in the spectral direction, resulting in 512 spectral channels. Data cubes are acquired by imaging each gas lamp many times (32 or more) over a period of several seconds, and the cubes are averaged to give a single frame of data that has a spectrum for each spatial position. These spectra exhibit many emission lines for each

lamp. Figure 4 shows the low-pressure Mercury spectrum taken with the Ocean PHILLS. The exact locations of known emission lines can be found in many references. By pairing up measured emission lines with known lines, a relationship is derived between channel number and wavelength of the center of the channel. This relationship has proven to be very linear, giving negligible quadratic and higher terms. Smile and keystone can be measured by the line position and width across the array. One unbinned pixel of rotation from edge to edge is evident in gas emission lamp data, with < 1 pixel of keystone and smile distortions.
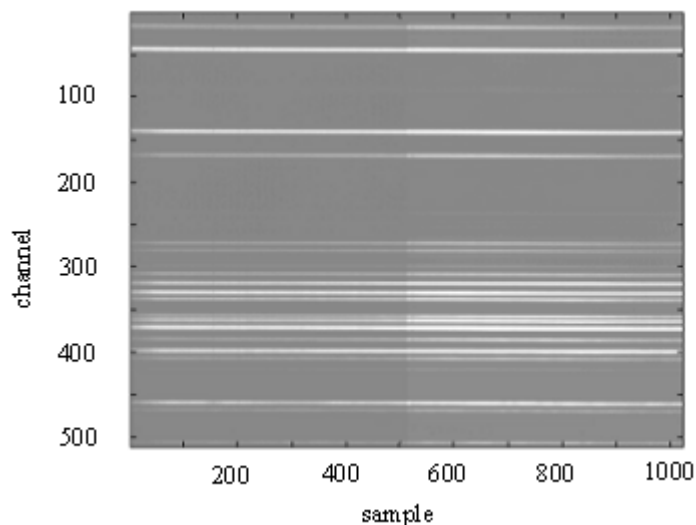
Figure 4. Image of a low pressure Mercury lamp showing 1024 spatial channels (horizontal) by 512 spectral channels (vertical dimension).

Frequently we have seen small (1-3 nm) discrepancies between the laboratory spectral calibration and the spectral position of known atmospheric features in our field data. Because the atmospheric correction algorithm is very sensitive to the spectral calibration, the wavelength calibration of field data are fine-tuned to match the locations of these strong atmospheric features. In particular, we adjust the channel wavelengths so that the resulting remote sensing reflectance spectra are correct around the Fraunhoffer line at 431 nm and the oxygen absorption peak at 762 nm.

3.3. Radiometric performance

The CCD is cooled to a stable temperature, but the temperature is maintained relative to the ambient temperature. To avoid errors due to changing dark current, a dark measurement is taken immediately following all PHILLS measurements (both calibration and field data). Typically this dark measurement of 1024 frames is averaged to provide a single dark frame that is subtracted from the illuminated measurement. The noise of the dark frame is approximately 30 counts.

The primary source used for radiometric calibration of the PHILLS is a 40 inch Spectraflect-coated integrating sphere (Labsphere, Inc., North Sutton, NH) containing 10 halogen lamps. The intensity of the output from the sphere at chosen lamp levels is determined by performing a transfer calibration from a NIST calibrated Field Emission Lamp (FEL). Because the sphere spectrum is red rich, a blue balancing filter is placed in front of the PHILLS lens to make the source more spectrally flat. In order to acquire calibration data over the largest possible dynamic range, data is typically taken with 1, 2, 3, 4, 6, 8, and 10 lamps

turned on. For each pixel on the CCD this data is used to calculate a quadratic relationship between data counts and radiance. The relationship is highly linear (Figure 5a), with the quadratic term typically accounting for less than 0.1% of the total radiance at each element of the CCD array. The overall efficiency of light collection by the system is higher at blue wavelengths than at red wavelengths, which results in a radiative calibration gain that is significantly higher at large channel numbers (red) than at small channel numbers (blue) (Figure 5b). The dynamic range, expressed in units of (W m^{-2} sr^{-1} nm^{-1}), is approximately proportional to the radiometric calibration gain shown in Figure 5b and is 2 to 4 times higher at red wavelengths than at blue wavelengths.

(a)

(b)
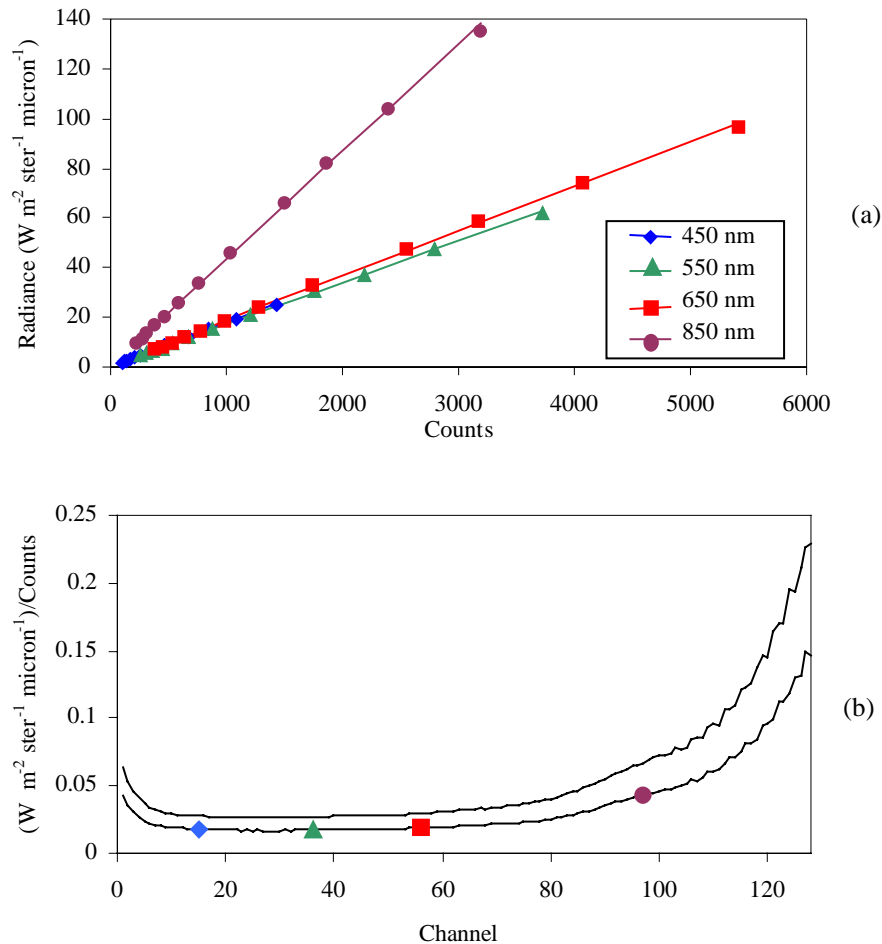
Figure 5. a) Linear fits to Ocean PHILLS radiometric calibration data for four selected wavelengths. b) Typical values of the radiometric calibration gain for the left (sample 488, top curve) and right (sample 517, bottom curve) side of the 1024 sample CCD. The spectral channels that correspond to the response curves shown in Figure 5a are marked with their legend labels.

The noise of the PHILLS was quantified by imaging the calibration sphere for 128 frames and analyzing the variation among the frames. The relationship between noise and signal expressed in terms of counts was found to be highly linear, making it possible to compute the SNR at any signal level. The slope of this relationship was found to be independent of

wavelength. Typical values of the SNR for bin-by-4 (4.8 micron) data are illustrated in Figure 6. The shape of the SNR plot generally follows the signal level. The high SNR in the blue for water scenes (Figure 6a) is an advantage with regard to extracting information from seawater and the sea floor where the blue signal dominates. In order to achieve this high SNR in the blue, the spectrometer was designed with a grating to optimize the SNR in the blue wavelength region at the expense of the red. This is a disadvantage with regard to trying to extract atmospheric information from the red wavelengths for the purposes of atmospheric corretion. This problem can be addressed by spatially binning the data to provide a higher signal from which to retrieve the needed aerosol/water vapor content values (these values change on a much larger spatial scale than the properties of the water). The SNR at red wavelengths is much higher when viewing terrestrial scenes (Figure 6b) due to the higher signal levels.
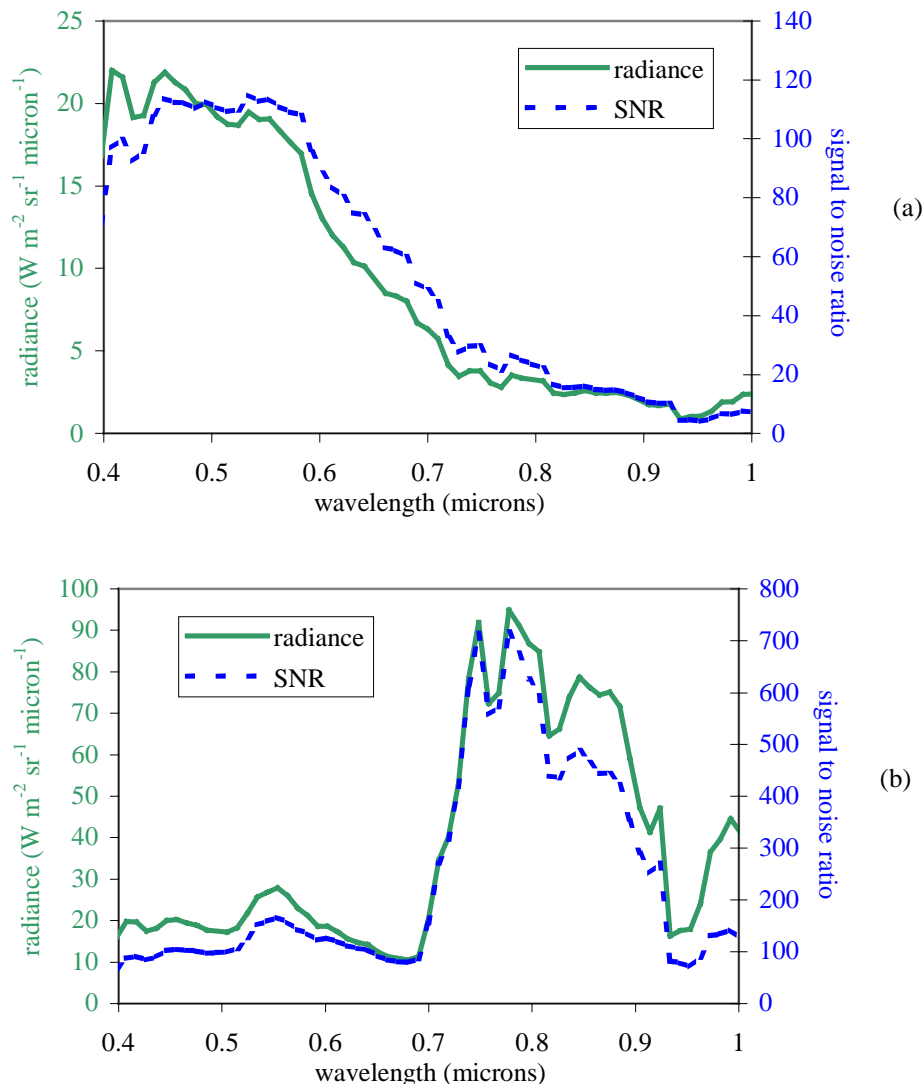

Figure 6. Typical at-sensor PHILLS radiance spectra and corresponding signal-to-noise ratios for bin-by-4 data from the LEO-15 site: (a) coastal water, (b) vegetated land.

4. Example results

Shown in Figure 7 is an RGB image (765 nm, 550 nm, and 450 nm) of remote sensing data taken by the PHILLS at the LEO-15 site on 31 July 2001 at 14:18 GMT. The approximate location of this image is 39° 31' 05" N and 74° 20' 47" W. The scene was collected from an Antonov AN-2 biplane (Bosch Aerospace, Huntsville, AL) traveling at an altitude of 2.6 km and an airspeed of 90 knots. The data were collected with an 17 mm lens, giving an on-ground pixel size of 1.8 m. The image shown is 1000 pixels across and 1024 pixels along-track (1.8 km x 1.8 km). The spectral calibration was adjusted using the position of the Fraunhoffer lines and the oxygen absorption line. Radiometric calibration was applied based on laboratory measurements using the FEL lamp and a Spectralon Plaque. The baseline stray light (Figure 3) was corrected for by assuming that 0.038% of the counts in each bin-by-4 spectral channel land in each of the other 127 channels. The data was then atmospherically corrected with Tafkaa, a new atmospheric correction program developed using a vector radiative transfer program [20,21]. Inputs to Tafkaa were a mid-latitude summer atmosphere model with a marine-type aerosol content of 0.122 atm-cm. The water content computed by Tafkaa was approximately 1.4 cm. Tafkaa accounts for the Gaussian shape of the PHILLS spectral response (Figure 3).
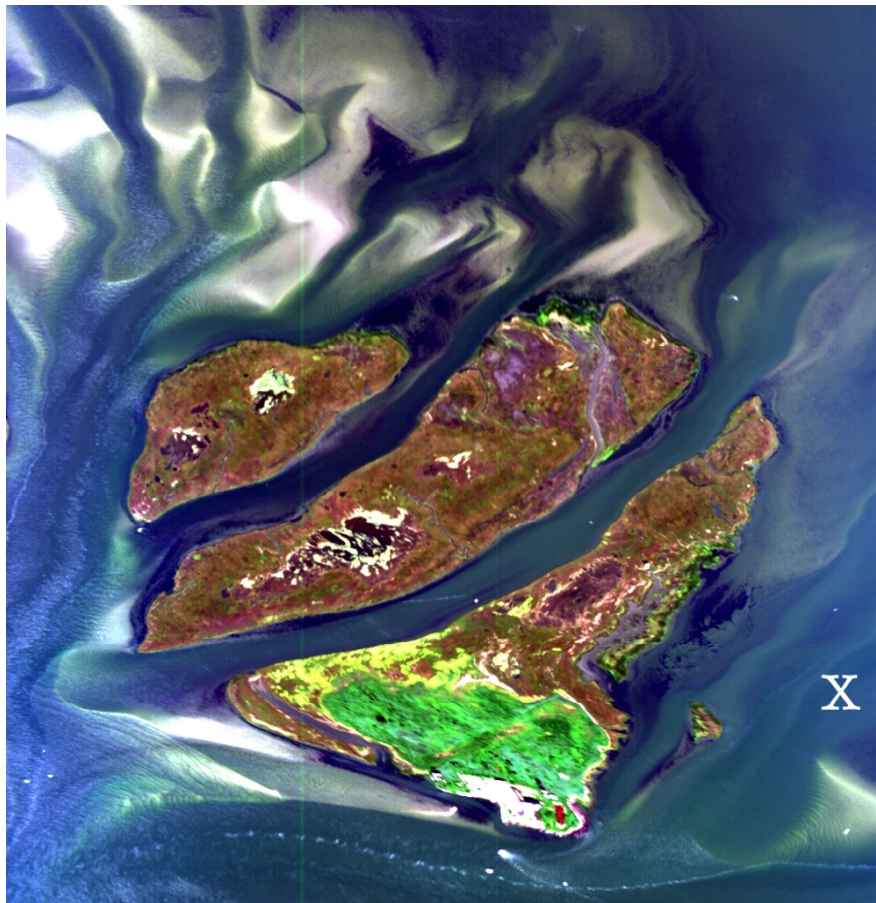

Figure 7. PHILLS image from the 2001 LEO-15 deployment (39 31 05 N and 74 20 47 W, 14:18 GMT, 31 July 2001.)

Shown in Figure 8 is an example of an atmospherically corrected spectrum from the point indicated in Figure 7. Also shown in Figure 8 is a spectrum taken during the overflight in the same general area with a hand-held spectroradiometer (Analytical Spectral Devices, Inc., Boulder, CO). The excellent agreement serves as an initial validation to our characterization, calibration, and atmospheric correction of PHILLS imagery.
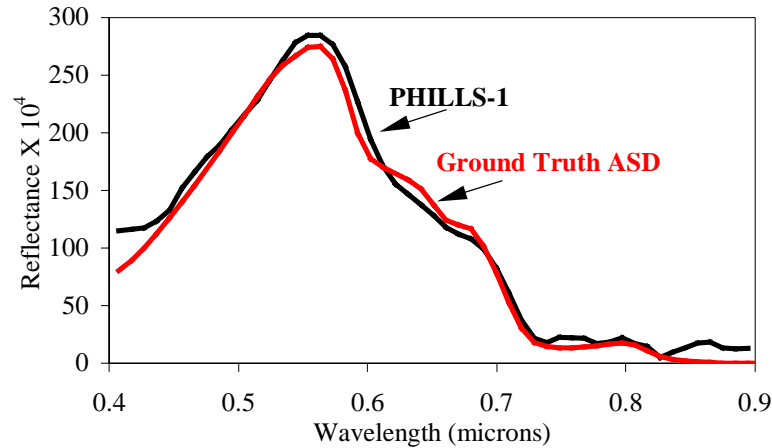

Figure 8: Atmospherically-corrected remote-sensing reflectance spectrum from the pixel indicated with an X in Figure 7 compared with a ground-truth measurement obtained with a hand-held radiometer at the site.

5. Conclusions

The Ocean PHILLS was specifically designed to produce high quality hyperspectral imagery of the coastal environment. Two key elements in this success are the VS-15 Offner spectrograph, which produces an image with minimal smile and keystone distortion, and the thinned backside-illuminated CCD cameras that have a high quantum efficiency in the blue. Both the spectral and radiometric responses of the instrument are highly linear. All of the components of the Ocean PHILLS are commercially available, making it possible for other groups to make similar instruments for a variety of applications.

We have demonstrated excellent agreement between atmospherically corrected remote-sensing spectra and ground-truth radiometric measurements. The next step is to use this data to calculate in-water properties using algorithms that have been developed based on shipboard and mooring measurements and models. The long-term goal is to be able to use hyperspectral data to extrapolate from these point measurements to characterize the water column and bottom properties of the shallow coastal ocean.